Evolution of damage in MoS_2-based dry film lubricants (DFLs) in fretting wear – the effect of DFL thickness and contact geometry

K. Barman[1], P.H. Shipway[1], K.T. Voisey*[1], G. Pattinson[2]

1. Faculty of Engineering, The University of Nottingham, United Kingdom, NG7 2RD.
2. Rolls-Royce plc, Derby, United Kingdom.

Abstract

Dry film lubricant (DFL) coatings are widely used to reduce coefficients of friction and damage in highly loaded contacts. This work investigates the behaviour of a commercially available MoS_2-based DFL in a cylinder-on-flat contact geometry with a fretting amplitude of 300 µm. Cylinders with radii of 15 mm, 80 mm and 160 mm along with DFL thicknesses between 12 µm and 86 µm were utilized. Three stages in the lifetime of the system were investigated; in the first stage, the DFL wore with a volumetric rate that was proportional to the number of cycles (under a given load), until the thickness of the DFL was reached. In the second stage, a thin low friction surface layer existed, with its durability being proportional to the contact pressure. In the third stage, metal-metal contact resulted in short-term instabilities in the coefficient of friction and the DFL system was said to have failed.

Keywords: fretting**,** coefficient of friction, wear, molybdenum disulfide, molybdenum disulphide, MoS_2, titanium alloy, Ti-6Al-4V

* Corresponding author: K.T. Voisey

1 Introduction

Mechanical vibration of highly loaded contacts can lead to fretting due to the resulting relative displacement between the two contacting bodies. Fretting can result in crack initiation and propagation (termed fretting fatigue) and also in loss of material at contact surfaces (termed fretting wear) [1]. In the fan blade/ disk dovetail in an aeroengine system (where both components are typically made from titanium alloys), both fretting wear and fatigue wear may occur due to relative motion at the contact [2-4]; in light of the poor tribological behaviour (high coefficient of friction and high rate of wear) of self-mated titanium alloys, a number of low-friction coatings having been developed with the purpose of reducing fretting damage in this particular application [5-7]. There is a desire for such anti-friction coatings to have extended lifetimes leading to lower numbers of maintenance interventions being required. Longer lifetimes are associated with lower rates of wear of the lubricant film itself, and the desire for low friction and long lifetime are often (but not always) complimentary, since low friction leads to a reduction in frictional energy dissipation and thus to reduced wear [8]. Such low-friction coatings are more generally referred to as dry film lubricants (DFLs) and are used in a variety of industrial applications to reduce the coefficient of friction where conventional liquid lubricants are ineffective or cannot be readily deployed [9, 10].

Molybdenum disulphide (MoS_2) is widely used as a dry film solid lubricant [6, 11] due to its laminar hexagonal structure which results in low coefficients of friction being observed [12, 13]; in many industrial sectors, the MoS_2 is often applied to a surface as a coating in the form of MoS_2 particles in a polymeric binder [14] (although MoS_2 can be utilized as a low friction material in a wide range of forms [15-19]). In the case of a polymer loaded with MoS_2 particles, the coating is often applied on top of a metallic bond layer (typically Cu-Ni-In) [20] which is itself deposited onto the component surface by thermal spraying. The Cu-Ni-In layer performs a number of functions, the most significant of which is that it is thought to act as a retainer for the polymeric DFL [3].

A number of investigations have been carried out to examine both the sliding and the fretting behaviour of MoS_2-loaded polymeric films [14, 15, 18, 19, 21-23], with thermal effects being observed to be significant in controlling behaviour in certain sliding test configurations. Fridrici et al. [24] investigated the effect of contact geometry on fretting life of a surface engineered system (Cu-Ni-In with a top coat of MoS_2) by comparing results from cylinder-on-flat contacts with flat-on-flat contacts. They determined a unique Wohler like master curve to predict the lifetime of a MoS_2 solid lubricant which proved to be independent of the contact geometry. Ye et al [14] examined the behaviour of 30 µm thick MoS_2-based DFLs in reciprocating sliding against an uncoated steel ball (the DFL was applied directly to a steel substrate with no soft metallic interlayer). In this case, both the wear coefficient and coefficient of friction were observed to increase with decreasing contact pressure, indicating a sensitivity to contact geometry.

Some data regarding the evolution of the coefficient of friction during fretting of MoS_2-containing DFL systems have previously been reported. A period of rapid change is often observed during an initial running-in stage which frequently produces an initial peak in the coefficient of friction; this is commonly followed by an essentially steady state secondary region during which the coating thickness progressively decreases (by wear) until a critical point is reached (the tertiary stage) where the coefficient of friction increases rapidly [25]. In recent work, Fouvry et al. [26] examined the fretting behaviour of a surface-engineered titanium alloy pair; both bodies had been shot peened, but on one of the bodies in the fretting pair, a coating system had been applied (Cu-Ni-In with a ~ 30 µm thick top coat of a MoS_2-containing epoxy resin). They observed that the friction coefficient at the beginning of tests was low and rose in a relatively steady manner to the point when coating failure occurred (which they defined as being the point at which the coefficient of friction reached 0.35). Kim and Korsunsky [1] also examined the behaviour of a similar system (sprayed Cu-Ni-In with an MoS_2-loaded epoxy layer) and observed that the development of the coefficient of friction depended upon the fretting amplitude (see Figure 1); with an amplitude of 75 µm, the coefficient of friction remained low for the duration of the test, whereas for larger displacement amplitudes (up to 300 µm), the coefficient of friction was initially high for a short period, and then was observed to fall to a minimum before rising steeply to a value associated with failure of the contact. As such, it is clear that the development of coefficient of friction is dependent (amongst other things) on the amplitude of fretting.

As well as the loss in thickness of the material, a number of researchers have also noted that degradation of such systems is also associated with the oxidation of MoS_2 to MoO_3 [8]. Indeed, Luo et al described the degradation of an MoS_2-containing epoxy resin in fretting as being a combination of abrasive wear, delamination and tribo-oxidation of the MoS_2 to MoO_3, with the latter transformation being responsible for a gradual increase in coefficient of friction from 0.2 to 0.3 throughout the fretting tests [27]. Similar increases in coefficient of friction associated with this chemical degradation of MoS_2 have been reported elsewhere [14, 28].

Kim et al. investigated the effect of two different coating thicknesses of a polymer bonded MoS_2 on a Cu-Ni-In metallic layer (total thicknesses of 50-80 µm and 100-150µm) and showed that durability of the system coating increased with increasing initial coating thickness [1]. Similarly, Zhou and Vincent [29] investigated the effect of initial coating thickness (5 µm and 50 µm) of polystyrene coatings on a steel substrate in fretting using a ball-on-disc arrangement. Here, a sudden increase in Coefficient of friction was observed after 10^3 cycles and 10^4 cycles for the 5 µm and 50 µm thick coatings respectively, with this being explained by the real initial contact area increasing significantly with increasing coating thickness. A large increase in contact area will decrease the induced shear stress, thereby helping to extend the life of coatings. Langlade at al. [30] conducted fretting tests with a DFL-coated steel, using two different types of DFL with a range of coating thicknesses. They observed that significant increases in life resulted from increases in the DFL thickness, with the increase in lifetime increasing more rapidly with increasing coating thickness at the lower thicknesses. For example, for a PTFE / thermosetting resin DFL, the lifetime was observed to increase by around a factor of ten as the thickness was increased from 6 µm to 15 µm (across a range of pressures from 850 MPa to 1200 MPa), but then only by a factor of less than three with a further increase in thickness to 22 µm. In addition, they also observed a substantial increase in the steady-state Coefficient of friction with increasing DFL thickness[1], although no hypothesis to explain this behaviour was offered.

In a contact where DFLs such as these may be used, the load to be carried is often a fixed parameter in the design, but the detailed geometry of the contact and the thickness of the DFL can be tailored to achieve optimum performance. Accordingly, in order to understand the influence of both DFL thickness and contact geometry on the DFL lifetime in a fretting (or reciprocating sliding) contact, the current work examines the fretting behaviour of a commercially available MoS_2-based polymeric DFL as these two parameters are varied in a cylinder-on-flat contact. Aggressive (high displacement amplitude [1]) fretting conditions were chosen to provide widest discrimination in behaviour. The evolution of the coefficient of friction throughout the sliding tests was monitored in both full tests and interrupted tests, along with characterization of the ensuing wear scars.

2 Experimental Methods

Fretting wear tests were conducted with a crossed cylinder-on-flat arrangement, as shown in Figure 2, with samples being machined from Ti6Al4V plate. The length of the contact (*w*) was 10 mm (determined by the width of the flat sample). Three different cylindrical sample geometries were used with radii (*R*) of 15 mm, 80 mm and 160 mm. Both specimens making up the fretting couple were grit blasted with aluminium oxide grit (Airblast, UK; grade NK36) with a

[1] There is some confusion in the paper with contradictions between the figures and the text. However, the text makes a clear statement in this regard, and thus it has been assumed that the figure (Figure 10) has been incorrectly labelled.

grit size 0.5 - 0.59 mm, yielding surfaces with a roughness (Ra) of around 2 µm. A SEM image of the as-blasted Ti6Al4V surface is presented in

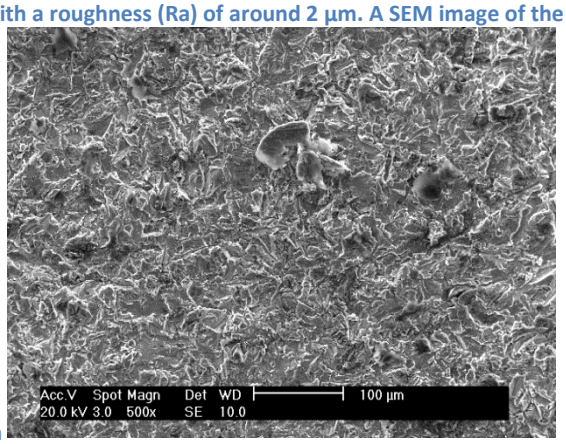

Figure 3. Immediately following grit blasting, a commercially available DFL polymeric paint (PL237 R2, Indestructible Paints, Birmingham, UK), in which the primary solid lubricant phase in the DFL was molybdenum disulphide (MoS_2), was applied using a spray deposition technique. To achieve the target DFL thicknesses, several passes of paint were used, with approximately ten minutes allowed between each successive pass. DFL coating thicknesses between 12 µm and 86 µm were examined. In each case examined, the DFL thickness was the same on both the flat and cylindrical specimens in the fretting couple.

The paint systems on the coated specimens were cured in an air-circulatory oven. Samples were placed in the oven initially at 100°C; the oven temperature was then immediately increased by 2 °C min^{-1} to 195 ± 1 °C where it was held for 2 h. The oven was then switched off and the cured samples remained in the oven whilst they cooled to room temperature. A PosiTector 6000 eddy current gauge (DeFelsko Corporation, USA) was used to measure the cured coating thickness, *t*, with a precision of ± 5 µm. Figure 4 shows plan-view SEM images of the as-cured DFL coating, where it can be seen that the film is a bonded agglomerate of individual MoS_2 particles.

For the fretting tests, specimens were mounted as shown in Figure 2 with fretting motion being applied perpendicular to the axis of the cylindrical specimen; a schematic diagram of the fretting rig used for the experiments is shown in Figure 5. A normal load, *P*, was applied, and relative displacement, *Δ*, between the cylindrical and flat specimens was achieved through control of an electromagnetic vibrator (EMV). The tractional force, *Q*, at the contact was measured as a reaction force by a piezoelectric load cell. The applied displacement amplitude was controlled via position measurement of the upper specimen mounting block using a linear variable differential transformer (LVDT).

A normal load, *P*, of 575 N was applied in the majority of tests (with a very small number conducted under loads of 2000 N). The flat specimen was fixed and the round specimen was fretted against it, moving with an applied displacement amplitude (*Δ**) of 300 µm at a frequency of 2.5 Hz. Using values for the Young's modulus and Poisson's ratio of 115 GPa and 0.342 respectively for the titanium alloy employed [31] allowed estimates of the maximum contact pressure for each geometry to be made, with these estimates being made through the use of standard Hertz theory and ignoring the presence of the DFL film itself in these calculations. For the cylinders of radius 15 mm, 80 mm and 160 mm, the calculated mean Hertzian contact pressures under the applied load of 575 N were 221 MPa, 96 MPa and 68 MPa respectively; these contact pressures form a range which spans the contact pressure of 125 MPa employed by Kim and Korsunsky [1]. The conditions for fretting (amplitude, frequency and

contact pressures) were selected since these have been indicated to be representative of those experienced in aerospace components where DFLs of this type are employed [1]. The load of 2000 N was only used in tests with cylinders of R = 15 mm (resulting in a mean Hertzian contact pressure of 413 MPa), with this being selected to allow the range of the mean contact pressures to be extended. The temperature and relative humidity of the environment were 20±3°C and 30±5% respectively. The fretting conditions used in this study are summarized in Table 1.

During the fretting tests, the tractional force and applied displacement were recorded at a rate of 200 measurements per fretting cycle, and were plotted to form fretting loops. A schematic diagram of a typical fretting loop is presented in Figure 6, showing a loop typical of those observed in this work where there were significant variations in the tractional force across the period of slip within each loop. The coefficient of friction (CoF) in each cycle was defined as follows:

$$CoF = \frac{Q^*}{P} \qquad \text{Equation [1]}$$

where *Q** is as defined in Figure 6. For each condition examined, tests to completion were terminated when the CoF reached a value of 0.7 (this value was chosen as it was the value observed after a low number (~ 6000) of cycles for fretting of uncoated Ti6Al4V samples in this configuration); these are termed *completed tests*.

It is recognized that the definition of the CoF (using the maximum tractional force) is strongly influenced by effects at the end of the traverse (such as build-up of ploughed material); another commonly used measure is that known as the energy coefficient of friction (ECoF) [32] which is based on the dissipated energy per cycle (E_d - as defined in Figure 6),

$$ECoF = \frac{E_d}{4\,P\,\delta} \qquad \text{Equation [2]}$$

with δ being the slip amplitude (distinct from the applied displacement amplitude, Δ^*); both of these parameters are illustrated in Figure 6. Although the ECoF was generally employed to describe the evolution of the coefficient of friction, the evolution of both CoF and ECoF are presented for one of the experimental runs so that the differences between these two measures can be understood; also, as previously stated, the in-test control system which was used to terminate tests was based upon the CoF rather than the ECoF.

Interrupted tests were conducted on selected samples from the test matrix, with the point of interruption being selected to be in region of interest, determined from the development of ECoF versus fretting cycles from the completed tests. Such tests were designed to facilitate a better understanding of the nature of the wear processes in the different stages.

Following testing, the geometry of the wear scars on the flat sample in each wear couple was characterized using a Taylor-Hobson Talysurf CLI 1000 contact profilometer. The central 8 mm region of the wear scar was scanned with 54 lines, all approximately parallel to the sliding direction and spaced 150 μm apart (see Figure 7). The average profile of the scar was formed by taking the average of the 54 line scans, and using the material outside the scar as a reference surface. The surfaces of the wear scars were also characterized using scanning electron microscopy (Philips XL30), using both secondary electron (SE) and backscattered electron (BSE) imaging along with energy dispersive X-ray

analysis (EDX) conducted at 20 kV and a working distance of 10 mm. In addition, X-ray photoelectron spectroscopy (XPS) was conducted on worn surfaces using a Kratos AXIS ULTRA with a mono-chromated Al Kα X-ray source (1486.6eV) operated with an emission current of 10 mA and an anode potential of 12 kV. A pass energy of 20 eV was employed with a step size of 0.1eV, with the area of analysis being defined by an aperture of 300 × 700 µm. A charge neutraliser was used to prevent sample surface charging. Analysis was conducted on the flat specimens from the fretting pairs, with a spacing of 0.5 mm between individual analysis positions stepping across the wear scar.

Selected worn samples were cross-sectioned using electro-discharge machining (EDM). Samples were cold-mounted in metallographic preparation resin after mounting, the surface was ground using different grades of silicon-carbide grinding paper, ranging from P600 to P1200 grit, followed by cloth polishing with colloidal silica. The cross section was imaged by SEM; panoramic images of the whole wear scar were produced by stitching individual images of the wear scar (taken at 500 times magnification) included the coating area on both sides as a reference surface. These images were then distorted to demonstrate certain features more effectively; each image was reduced to a tenth of its original length in the horizontal axis, whereas the length in the vertical was preserved.

3 Results

Figure 8 shows the development of the coefficient of friction with increasing cycles from a single test, illustrating the difference between the CoF and the ECoF. The general form of the evolution in frictional behaviour is described equally well by the ECoF and the CoF, but the ECoF is generally lower than the CoF since it represents the average behaviour across the loop (as opposed to the CoF which utilises the maximum tractional force recorded within the loop). The ECoF is thus less sensitive than the CoF to the influences of geometrical changes in the wear scar which can cause end-peaks in fretting loops [33], and thus the ECoF will be used from hereafter in this paper.

It is recognised that the applied displacement amplitude (Δ*) rather than the contact slip (δ) is controlled in the experimental system (see Figure 6 for definition of terms). The loops can be interrogated to yield the system stiffness (part of which may be attributed to the stiffness of the contact itself); the stiffness (S) is given by the slope of the part of the fretting loop where the contact is not sliding (as illustrated in Figure 6). Some variations in contact stiffness were observed as the geometry and DFL thickness were varied, with values between 80 MN m^{-1} and 140 MN m^{-1} being recorded. Even for the most compliant system at the highest tractional forces exerted in a loop (around 1400 N in the most extreme condition when the CoF = 0.7 and P = 2000 N), the elastic deformation (i.e. Δ* - δ) is around 18 µm, which is less than 6% of the applied displacement amplitude (Δ* = 300 µm). As such, the reciprocating slip amplitude (δ) will be assumed to be the same for all combinations examined.

Figure 9 shows the development of the ECoF with number of cycles for three DFL thicknesses (t) across the range examined on contact pairs with R = 15 mm; in each case, the development of ECoF in two individual tests is presented to illustrate the repeatability of the evolution of frictional behaviour. Across the range of thicknesses, three stages in the evolution of frictional behaviour are apparent; these will be described at this stage to facilitate more efficient description of the evolution of ECoF with cycles throughout the paper. An example of the ECoF evolution with number of cycles is presented in Figure 10, along with a categorization into three stages as follows: in Stage I, the coefficient of friction at first rises, and then slowly falls or remains approximately constant. At the start of Stage II, the coefficient of friction falls (generally quite rapidly) until a minimum point is reached;

the ECoF then rises slowly and steadily from this minimum point until it starts to exhibit short term instability; this is defined as the end of Stage II. In Stage III, the coefficient of friction continues to exhibit short term instability (periods of high friction) but also continues to rise until the test is terminated. The total number of cycles in each stage is thus defined as N_I, N_{II} and N_{III}, where the subscript refers to the appropriate stage.

3.1 Damage mechanisms throughout the system lifetime

In order to understand the nature of the evolution of the damage which corresponds to the changes in ECoF with number of cycles, a number of interrupted tests were conducted with the same geometry and DFL thickness as described in Figure 10; the evolution of ECoF with cycles is presented in Figure 11 for both the same test as shown in Figure 10 as well as two of the interrupted tests (following 5k cycles and 36k cycles); the high level of reproducibility in the development of the ECoF over the three tests can be observed. Figure 11 shows profiles across example wear scars, with the maximum depth of the wear scar as a function of number of cycles for all the tests conducted being presented in Table 2. It can be seen that in stage I, the wear scar gets deeper, and is approximately as thick as the DFL layer itself at the end of Stage I. In Stage II, the scar depth is just a little deeper than the original DFL thickness, whilst by the end of Stage III, the scar is much deeper than the original DFL thickness. The distorted low magnification SEM images presented in Figure 12 show cross-sections through the wear scar at three points within the scar evolution which correspond to the profiles presented in Figure 11b (these micrographs are presented in a form where the vertical magnification is ten times that of the horizontal magnification since this provides a clearer visualisation of the damage incurred). It can be seen that after 5k cycles (Figure 12a), significant wear of the DFL has occurred to approximately a third of the DFL thickness. Following 36k cycles (Figure 12b), the coating has been largely removed from the centre region of the scar, but with areas towards both edges of the scar where a small quantity of the DFL can be seen which appears to be retained by the surface roughness of the substrate. Following 68k cycles (Figure 12c), significant damage and material removal from the substrate can be seen.

Figure 12 also shows higher magnification images of cross-sections through the wear scars; it can be seen that after 5k cycles (Figure 12b), the outer surface of the DFL has been modified, but that these changes are quite subtle and only affect a layer about 2 μm in thickness. The EDX results from the bulk and surface regions of the DFL indicate very little change in chemistry at the surface and that there is no evidence of any elements from the substrate at the wear surface by this stage. After 36k cycles (Figure 12d), there is evidence of some remnants of the DFL remaining on the surface, but it can be seen that this layer exhibits a generally homogeneous brightness (in contrast to the cross-section shown in Figure 12b where the binder and MoS_2 can be clearly distinguished due to difference in brightness in BSE imaging). EDX analysis shows that this surface is chemically not very different from the original DLF. In Figure 12f, it can be seen that no traces of the DFL exist, a fact which is confirmed by the results of the EDX analysis.

Figure 13 shows plan view images of the wear scars following the tests indicated in Figure 11a, with Table 2 detailing results from large-area EDX analyses of the same wear scars; the presence of molybdenum indicates the presence of the DFL in the wear scar, whereas the presence of titanium indicates the presence of the Ti6Al4V substrate. It can be seen that there is no evidence that the substrate has been exposed within Stage I, but that by 31% through stage II, there is clear exposure of the substrate; the ratio of titanium to molybdenum tends to increase with number of cycles through Stage II (i.e. the DFL fraction reduced and the substrate fraction increased); by the end of Stage III, all evidence of the molybdenum-containing DFL has been removed. In addition, Figure 14 provides

elemental line profiles across the wear scar following 36k cycles (i.e. in stage II) generated via the more surface-sensitive XPS analysis technique.

After 5k cycles, Figure 11b and Figure 12a indicate that there has been no penetration of the DFL to the substrate. Accordingly, it is clear that Figure 13a and Figure 13b show the worn surface of the DFL itself, some regions of which exhibit a smooth surface associated with the rubbing action of the fretting process (linked to the subtle modification of the surface region observed in Figure 12b), whereas other regions exhibit a much rougher surface.

After 36k cycles, Figure 11b and Figure 12c indicate that the DFL has been penetrated; specifically, in addition, data in Table 2 indicate that after this number of cycles, the surface is still dominated by the DFL (the molybdenum content is still a large fraction of that measured in the unworn DFL), but there is evidence of a small fraction of titanium alloy in the surface material (the measured titanium content via EDX analysis is ~ 9 wt.%, which equivalent to ~ 4.5 at%). The micrographs in Figure 13c and Figure 13d also indicate that the surface is made up of different regions; those with a lower brightness still have evidence of DFL being present, whereas those with a higher brightness are regions where the DFL has been removed, just leaving substrate exposed. Ploughing marks can be seen running across the surface, but the surface is generally quite smooth indicating that wear has been mild at this point. However, the XPS data (Figure 14) show a much lower titanium content across the surface (~ 1 at%), which indicates that the surface material which appears titanium-rich via BSE imaging and EDX analysis is in fact covered by a layer which is rich in carbon, oxygen, molybdenum and sulphur, but that this layer is thin enough that it is detected by XPS analysis but not by EDX analysis and BSE imaging. Moreover, the XPS trace across the wear scar (Figure 14) indicates a substantial reduction in carbon in the wear scar with an increase in molybdenum and sulphur, indicating that the surface of the wear scar is preferentially enriched in MoS_2 by the wear process itself.

After 68k cycles, Figure 11b and Figure 12e indicate that the DFL has been entirely removed, with wear to a depth twice that of the original DFL coating thickness. In addition, Table 2 indicates that there is a complete absence of molybdenum from the EDX analysis. The micrographs in Figure 13e and Figure 13f indicate significant surface disruption, as is commonly observed in the fretting of titanium alloys.

3.2 The effect of DFL thickness and fretting pair geometry

The same general trends in the evolution of frictional behaviour are also observed for the other contact geometries (R = 80 mm and R = 160 mm) across the range of DFL thicknesses (see Figure 15). Only in the test conducted with a DFL of thickness of 62 µm on a 160 mm radius cylinder was it difficult to identify the boundary between Stages II and III, since Stage III appeared to begin before Stage II had fully developed.

Results reported in Section 3.1 relating to the smaller radius cylindrical samples in the fretting pairs (R = 15 mm) indicate that Stage II is associated with a period where the DFL has been largely removed with some exposure of titanium alloy substrate (which increases as stage II develops). To confirm that this conclusion was valid for other thicknesses of DFL and other contact radii, tests interrupted towards the start of Stage II were conducted as indicated in Figure 16 (R = 80 mm, t = 12 µm and 62 µm). In both cases, the evolution of the ECoF (up to the point where the tests were terminated) was very similar for the completed and interrupted tests (again indicating reproducibility of behaviour). Depth profiles of the wear scars resulting from these interrupted tests (Figure 17) show that in both cases, the wear scar depth in Stage II was slightly larger (within the variability of the

surface roughness of the substrate before DFL deposition) than the DFL thickness. EDX analyses of the worn surfaces again reveal their mixed substrate/ DFL makeup, with Ti at 20 wt% and Mo at 21 wt% (t = 12 µm) and Ti at 27 wt% and Mo at 27 wt% (t = 62 µm). These observations together indicate that the identification of Stage II with a period where the surface in contact is comprised of a combination of the DFL and the metallic substrate material has general validity.

A range of combinations of DFL thickness and contact geometry have been examined with a constant load of 575 N. Two additional tests were conducted under the higher load of 2000 N, both with R = 15 mm but towards the extremes of the thicknesses considered (t = 25 µm and t = 86 µm). The full experimental programme is summarised in

Table 3 along with the durations of the three stages for each of the tests; these durations for tests conducted with an applied load of 575 N are also presented in Figure 18. From examination of these data, the following general observations can be made:

(i) For each contact radius, R, the total test duration is dominated by Stage II and III at low values of t, but Stage I becomes a very significant fraction of the total lifetime for larger values of t;
(ii) the duration of Stage I increases both with increasing t and increasing R, although the dependence upon t is much more significant than that upon R;
(iii) the duration of Stage II increases slowly with R, but at each contact radius, it exhibits no clear dependence upon t;
(iv) at the start of stage II, a significant decrease in the ECoF is observed until a minimum is reached; the rate of this reduction decreases significantly for t = 62 µm for the two larger values of contact radius, R;
(v) for each contact radius, R, the duration of Stage III shows a large increase at a specific value of t; below this value of t, the duration of Stage III is broadly independent of t;
(vi) the minimum value of ECoF in stage II is higher for the two larger values of R than it is for R = 15 mm; at the two larger radii, the minimum value of ECoF also increases as t increases;
(vii) the higher applied load of 2000 N resulted in a significant reduction in the duration of all three stages when compared to equivalent tests conducted with an applied load of 575 N.

4 Discussion

4.1 Durability of surface engineered systems

There has been great success over recent years in being able to link fretting wear damage in homogeneous materials with the energy dissipated in the contact (the wear volume is readily measured following testing, and the energy dissipated is derived from the fretting loops). In a homogeneous material, the behaviour and failure of the system and the mechanisms of damage accumulation do not depend strongly upon the depth to which material has been removed, and thus such methodologies have generally been observed to be very robust.

However, such a methodology is not as readily applied to a surface engineered system, where the behaviour and failure of the system, along with mechanisms of damage are dependent upon the depth to which material has been removed. Failure is often associated with the complete removal of a surface engineered layer, and accordingly, the wear volume does not uniquely define whether failure has occurred; as such, system failure cannot be linked intrinsically to the frictional energy dissipated. As such, a model is required which circumvents this issue. Fouvry and co-workers have proposed such a model [34] which has been used to rationalise coating lifetime in terms of the maximum frictional power density dissipated in the contact [24, 35]. The model is complex, partly because it does not specifically address the various physical stages in the lifetime of the DFL system. In the current work, the durations of the various stages will be considered separately.

4.2 Duration of Stage I

It has been shown that in Stage I, the DFL is being worn away and that by the end of Stage I, the DFL has been removed to the point where the metallic substrate is exposed. A basic geometrical model of this situation is presented in Figure 19a, which represents a coated cylinder of radius R in contact with

a coated flat, with the coatings on both being of thickness t. To allow the substrate of the two bodies to come into contact requires removal of coating from both the cylinder and flat (see Figure 19b).

The contact semi-width observed on the flat sample will lie somewhere between w_i and w_o (see Figure 19b), depending upon exactly where the wear has occurred. These two are given by the following equations:

$$b_i = \sqrt{R^2 - (R-t)^2} = \sqrt{2\,R\,t - t^2} \qquad \text{Equation [3]}$$

$$b_o = \sqrt{(R+t)^2 - R^2} = \sqrt{2\,R\,t + t^2} \qquad \text{Equation [4]}$$

For the range of values of R and t employed in this work, the difference between w_i and w_o is never more than 0.2%, and accordingly, the total contact width observed on the flat specimen, $W_s$can be approximated by:

$$B_s = b_i + b_o + 2\,\delta \qquad \text{Equation [5]}$$

The widths of wear scars on a range of flat samples where the tests had been terminated soon after the beginning of Stage II were measured. To test the hypothesis that Figure 19b is representative of this situation, the measured scar width was plotted against the idealized scar width, B_s (from Equation 5); Figure 20 shows the correlation between the measured and idealized scar widths. There is reasonable correlation between these two (although the correlation deteriorates as wear progresses) which further adds to the evidence that Stage I of the failure process is defined by the almost complete removal of the DFL by wear.

The idealized model has been shown to have merit, and can thus be further employed in the analysis of the duration of Stage I. According to the model (Figure 19), the combined cross-sectional area of DFL which needs to be removed to allow the substrate of the two bodies to come into contact is given by the chordal area of a circle of radius R and depth 2 t. This chordal area, A_I, is related to these two parameters by the following equation:

$$A_I = R^2 \cos^{-1}\left(\frac{R-2\,t}{R}\right) - (R-2\,t)\sqrt{R^2 - (R-2\,t)^2} \qquad \text{Equation [6]}$$

It is recognised that since the slip amplitude is δ, then the total volume of DFL which will be displaced in reaching this situation, V_I, is given by:

$$V_I = (A_I + 2\,\delta\,t)\,w \qquad \text{Equation [7]}$$

where w is the contact line length (see Figure 2).

If it is assumed that the volume of DFL removal in Stage I is proportional to the number of cycles and the applied load, then the following equation will apply:

$$V_I = k_I\ N_I\ P \qquad \text{Equation [8]}$$

To test the validity of this assumption V_I is plotted against N_I for all the tests conducted under a load of 575 N as shown in Figure 21. It can be seen that the correlation is reasonable across the range

across the range of values of R and t. Fitting these data results in the following relationship for Stage I:

$k_I = 0.15 \times 10^{-6}$ mm^3 cycle^{-1} N^{-1} Equation [9]

To enable this to be presented in the manner (Fig 22) of an energy wear coefficient requires the relationship between the cumulative energy dissipated in Stage I and duration of Stage I to be defined. The total dissipated energy in a stage is simply the sum of the energy dissipated in the individual cycles in that stage, (E_d – see Figure 6). These data are available for all the tests conducted, and a best fit yields 0.347 J cycle^{-1} under the test conditions selected. Accordingly, the volumetric wear coefficient for Stage I can be determined as follows:

$k_I^E = 3.9$ kJ mm^{-3} Equation [10]

4.3 Duration of Stage II

Results indicate that the majority of the thickness of the DFL has been removed by the start of Stage II. Whilst EDX analysis of the wear scar surface at the start of Stage II (Table 2) indicates that elements from both the titanium alloy substrate and the DFL are detected, the XPS data indicate that there is a thin surface layer rich in carbon, molybdenum and sulphur, which results in the low coefficient of friction which characterizes Stage II. It is clear from the ECoF that significant direct contact between the titanium alloy substrates in the contact pair is not occurring (such contact is typically associated values of ECoF of > 0.7). It is clear that this low friction is only achieved with a layer which has some metallic content, and is not a feature of the DFL itself.

In light of these observations, is proposed that the nature of the surface in Stage II will be independent of the thickness of the DFL originally applied (since it has been removed by the start of this stage and cannot therefore exert an influence). However, degradation of this surface clearly occurs, and eventually, direct contact between the titanium alloy substrates takes place, with the associated high coefficient of friction which defines the end of the stage. The Archard wear equation in its normal form indicates that wear volume is proportional to applied load; this same proportionality can be written in terms of the depth to which material is removed and contact pressure, with this being more appropriate in the consideration of a surface engineered system when failure is often associated with removal of material to a certain critical depth (namely, the thickness of the surface engineered layer). Accordingly, it is proposed that the duration of Stage II (N_{II}) will be inversely proportional to the contact pressure, p, as follows:

$$N_{II} = \frac{c}{p}$$ Equation [11]

where c is a constant. Given that it has been shown majority of the DFL has been removed by the time Stage II commences, it is proposed that the mean Hertzian contact pressure between the substrates (which is dependent upon both the contact geometry and the applied load) is the appropriate pressure to use; in the calculation of the contact pressure calculation, only the substrates are considered, since it is assumed that the DFL is largely absent in Stage II.

In Figure 23, the duration of Stage II (N_{II}) is plotted against the reciprocal of the mean Hertzian contact pressure; although there is considerable spread in the values of N_{II} at each contact pressure examined, the general concept of the proportionality in Eq. 11 is supported in that the two higher

pressure cases (R = 15 mm and P = 2000 N; R = 15 mm and P = 575 N) exhibit much shorter Stage II durations than the two lower pressure cases (R = 80 mm and P = 575 N; R = 160 mm and P = 575 N). Using these data, it can be shown that c = 6.5 × 10^6 cycle MPa. However, it must be recognized that although there is broad correlation, the correlation is not strong; specifically, at the two lower pressures, there is a significant range of values ofN_{II}, with one value much higher than the rest in each case. These observations indicate that there are other factors which influence N_{II} which are not addressed in this analysis, and have (as yet) not been identified.

4.4 Duration of Stage III

At the beginning of Stage III, the low-friction surface which characterizes Stage II is beginning to fail, with some substrate-substrate contact occurring. This removal of the low friction Stage II surface continues through Stage III until enough has been removed that the CoF reaches the value of 0.7, whereupon the test was terminated. At the end of Stage III, the depth of the wear crater is much larger than the original DFL thickness; in addition, EDX analysis of such surfaces provides no evidence for the presence of any elements associated with the DFL (Table 2). Inspection of the values of N_{III} (presented in

Table 3) indicate a wide variation of durations across the tests conducted. As previously noted in the summary of observations at the end of Section 3.2, at each contact radius, the duration of Stage III shows a large increase at a specific value of t, indicating that N_{III} has a dependency upon the thickness of the DFL, despite the DFL having been largely removed by the end of Stage I; currently this dependence of N_{III} upon t is not understood. However, it should also be noted that below the critical value of t where the significant increase in N_{III} is observed, then N_{III} is broadly independent of t.

Given the discussion regarding the duration of Stage II, one could argue that N_{III} would be expected to again be proportional to the reciprocal of the contact pressure. Figure 24 shows that, whilst there is some evidence that N_{III} decreases as the contact pressure increases, the correlation proposed is not supported by the data.

4.5 Lifetime of DFL system

DFLs are typically applied to components in service to reduce the coefficient of friction and as a means to avoid component (substrate) damage. In a service environment where DFLs such as these are deployed, a DFL should be replaced before the end of Stage II so that significant damage to the component (substrate) does not result. In this work, it has been shown (Equation 8) that the duration of Stage I is proportional to the volume of DFL that needs to be displaced (worn away) to get to a position of substrate-substrate contact. This volume can be readily calculated if the DFL thickness and contact geometry are known; the duration of Stage I can be calculated as the wear coefficient has been evaluated (Equation 9). This is followed by Stage II where a complex metal-DFL surface results in very low coefficients of friction. The duration of Stage II can now be predicted (Equation 11), noting that it is inversely proportional to the contact pressure. It is noted that in Stage III, substrate damage is accruing rapidly and the coefficient of friction is rising and varies in a stochastic manner, and thus entry in to this region should be avoided.

4.6 Comparison with previous quantitative work

There are few studies in the literature where attempts to quantify wear coefficients (and thus provide a basis for predictions of lifetimes) of such DFL systems have been attempted. However, recently Fouvry and Paulin [26] presented data regarding a 30 µm thick polymer bonded MoS_2 DFL fretting against Ti6Al4V under a wide variety of geometries, normal loads and fretting amplitudes. In the system that they examined, the DFL was deposited onto a Cu-Ni-In sublayer (150 µm thick) which was deposited onto a titanium alloy substrate. They derived a volumetric fretting energy parameter of ~ 66 kJ mm^{-3} for the system, but this was derived from an energy per unit area and an assumption that this could be converted to an energy per unit volume for removal of the MoS_2-containing DFL simply by dividing through by the DFL thickness. In addition, it is clear that the evolution of the coefficient of friction was very different; for contact pressures below 500 MPa (applicable to the tests carried out in this work), the behaviour associated with Stages I to III was not observed in the same form, with instead a gradual increase in friction being observed until the surface concentration of Cu-Ni-In reached around 55%, whereupon the coefficient of friction increased more rapidly. As such, it is clear that prior to this point being reached, the surface layer was composed of a mixture of the MoS_2-containing polymer and the Cu-Ni-In, with the Cu-Ni-In clearly being observed to make up part of the surface at relatively small fractions of the number of cycles required to reach the critical point.

Fouvry and Paulin derived an energy-based wear coefficient of 66 kJ mm^{-3} for the degradation of the system. This can be compared with the value of 3.9 kJ mm^{-3} derived in the current work which relates only to Stage I (i.e. the removal of the bulk of the DFL). The significant differences can be accounted

for by the fact that the work of Fouvry and Paulin considers a system with a sprayed C-Ni-In underlayer, and that the value of wear coefficient in that work is a convolution of all aspects of wear, whereas these have been separated into stages in the current work.

5 Conclusions

The degradation of a MoS_2-based DFL on a titanium alloy substrate has been shown to take place in three distinct stages. In the first stage, the polymer-based DFL wears away until the substrate starts to come into contact; during this stage the coefficient of friction falls slowly. In the second stage, there is initially a significant reduction in the coefficient of friction; this is linked to the formation of a surface made up of both features of the metallic substrate and the DFL. There is an enhanced level of MoS_2 on the surface; very little metallic material is present at the very surface, but the low friction material which covers the metallic substrate is very thin. After a number of cycles, this protective low friction material is no longer effective, and true metal-to-metal contact begins to take place with a commensurate increase in the coefficient of friction. In the first stage, the volume of coating removed is observed to be proportional to the number of cycles; as such, the duration of this stage can be estimated based upon the geometry of the contact and the DFL thickness. The duration of the second stage was seen to be inversely proportional to the contact pressure; as such, this can be estimated based upon a knowledge of the geometry of the contact.

6 Acknowledgements

Rolls-Royce plc is acknowledged for their funding of this research.

7 Tables

Table 1: Fretting test conditions

Normal Load (N)	575, 2000
Frequency (Hz)	2.5
Displacement amplitude (µm)	300
Room temperature (°C)	20±3 (ambient)
Relative humidity (%)	30±5 (ambient)

Table 2 Analysis from surface of wear scars (R = 15 mm, t = 50 µm) for tests interrupted at various points. The point of interruption is described by position in stage (defined by numbers of cycles). EDX analysis of titanium and molybdenum representing the substrate and DFL respectively (elements included in the EDX ZAF analysis: Ti, Al, V, Mo, S, C, O). The maximum depth of wear scar is also presented.

N / kcycles	Stage position	Ti / wt%	Mo / wt%	Depth of scar / µm
5	24% through Stage I	0	38	14
10	49% through Stage I	0	30	29
20	98% through Stage I	0	26	61
30	31% through Stage II	17	25	65
36	50% through Stage II	9	28	64
40	63% through Stage II	41	9	66
68	100% through Stage III	49	0	125

Table 3 Durations of Stages I, II and III in reciprocating sliding tests as a function of R, t and P

R / mm	t / µm	P / N	N_I / 1000	N_{II} / 1000	N_{III} / 1000
15	12	575	0.5	33.1	14.8
15	25	575	1.7	21.8	14.5
15	33	575	0.9	38.5	18.7
15	50	575	20.5	31.0	16.5
15	62	575	23.4	33.6	21.7
15	86	575	65.2	34.2	64.2
80	12	575	2.1	55.9	19.5
80	25	575	8.7	66.2	27.8
80	62	575	102.0	93.0	99.0
160	12	575	3.1	69.8	19.8
160	25	575	8.4	79.6	29.0
160	62	575	127.0	73.0	66.2
160	86	575	190.0	148.0	48.8
15	25	2000	0.7	7.8	4.2
15	86	2000	0.9	9.7	4.9

8 Figures

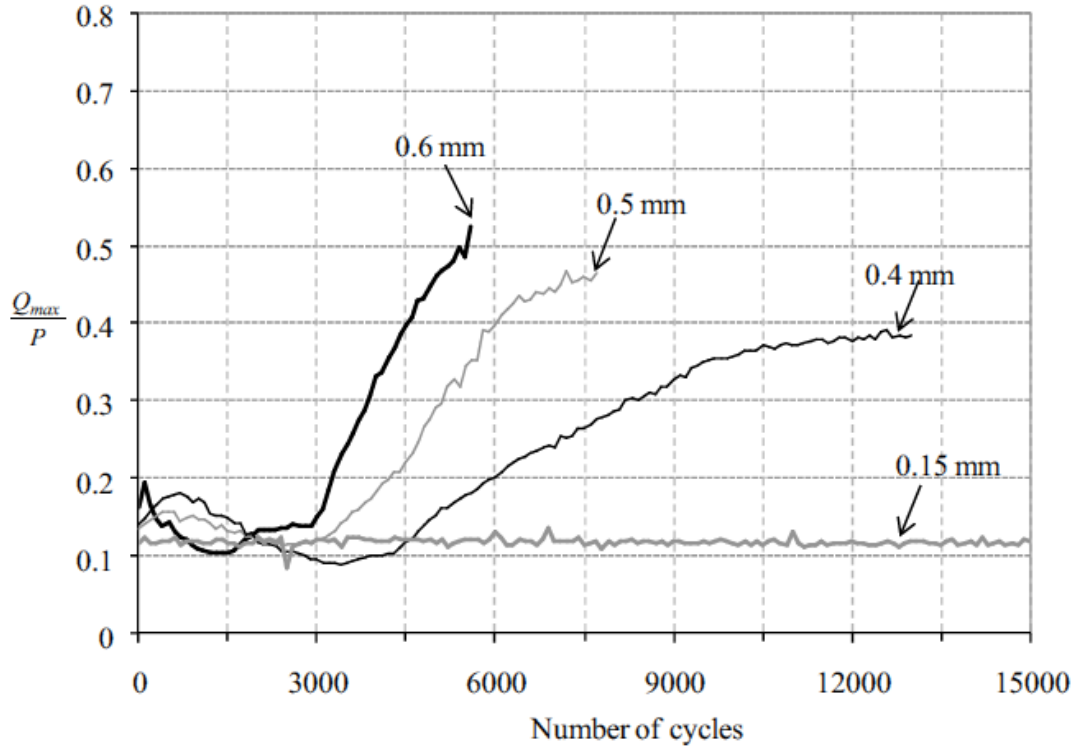

Figure 1: Development of the coefficient of friction with number of cycles for a DFL system as a function of peak—to-peak slip in the contact (as indicated on the figure). Figure reproduced from [1].

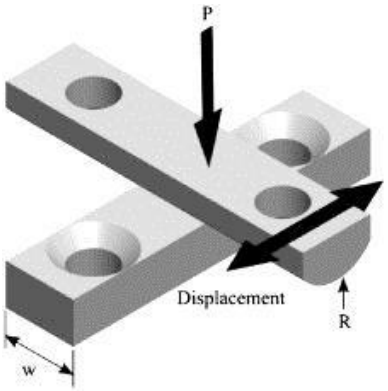

Figure 2: Cylinder-on-flat specimen setup for the fretting test [18], where W= 10 mm, R= 15 mm, 80 mm or 160 mm and P = 575 N or 2000 N

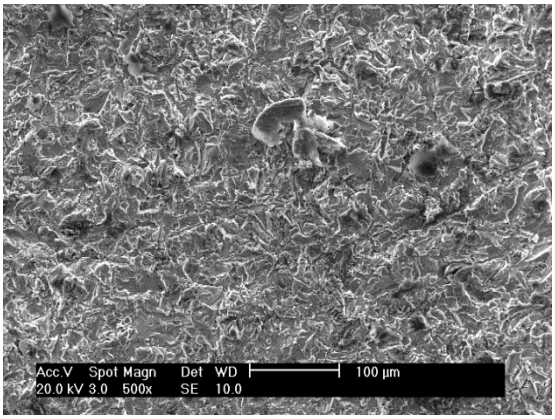

Figure 3 Secondary electron SEM image of the surface of grit-blasted Ti-6Al-4V before application of the DFL.

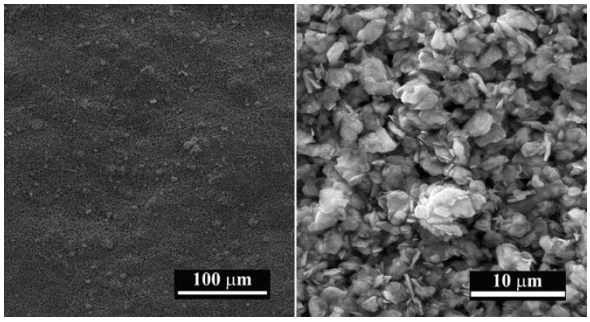

Figure 4: Low magnification (left) and high magnification (right) SEM micrograph of the surface of the as-cured DFL paint coatingMoS_2

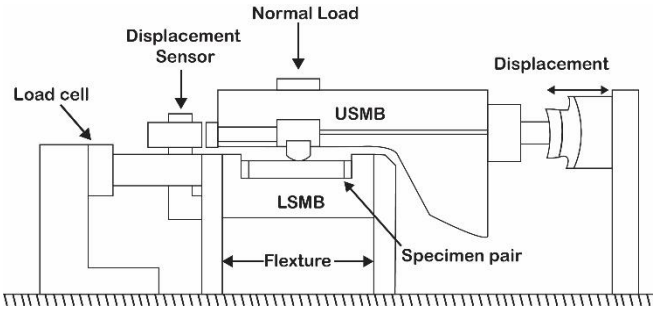

Figure 5: A schematic diagram of the fretting rig

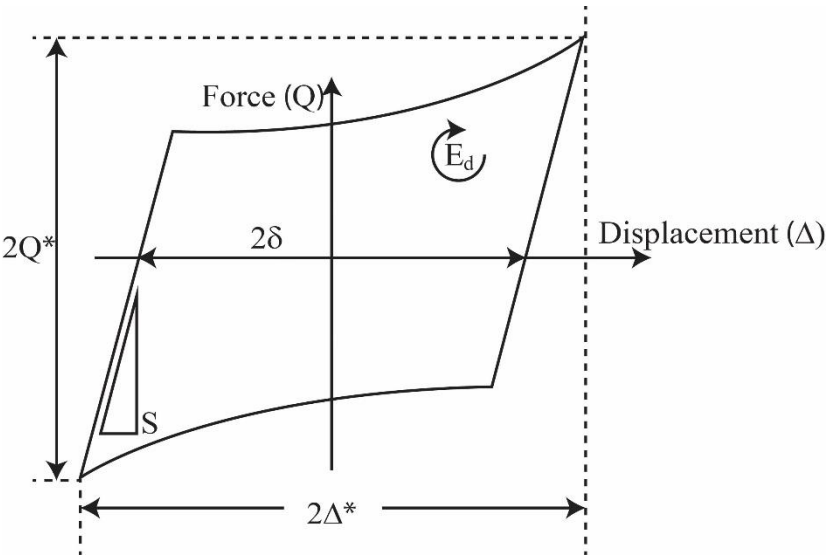

Figure 6 Schematic diagram of a fretting loop showing and increase in tractional force Q as slip proceeds (after [33]).

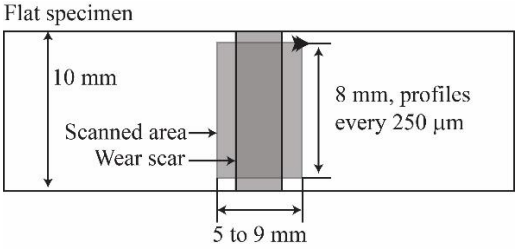

Figure 7 Schematic diagram illustrating the details of the profilometry procedures for the flat fretting specimens.

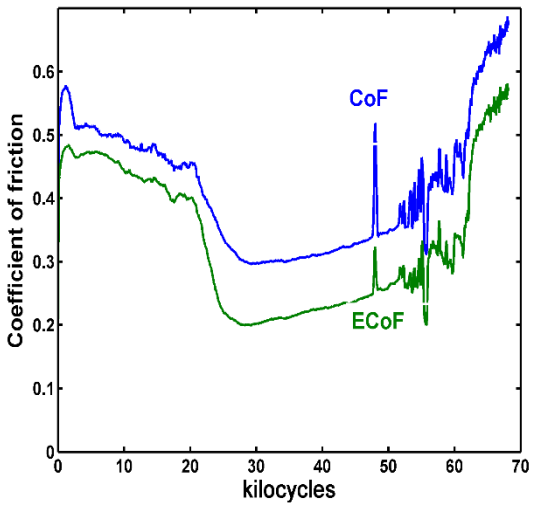

Figure 8 Evolution of both CoF and ECoF from the same test (R = 15 mm, t = 50 µm) which was run until coating failure.

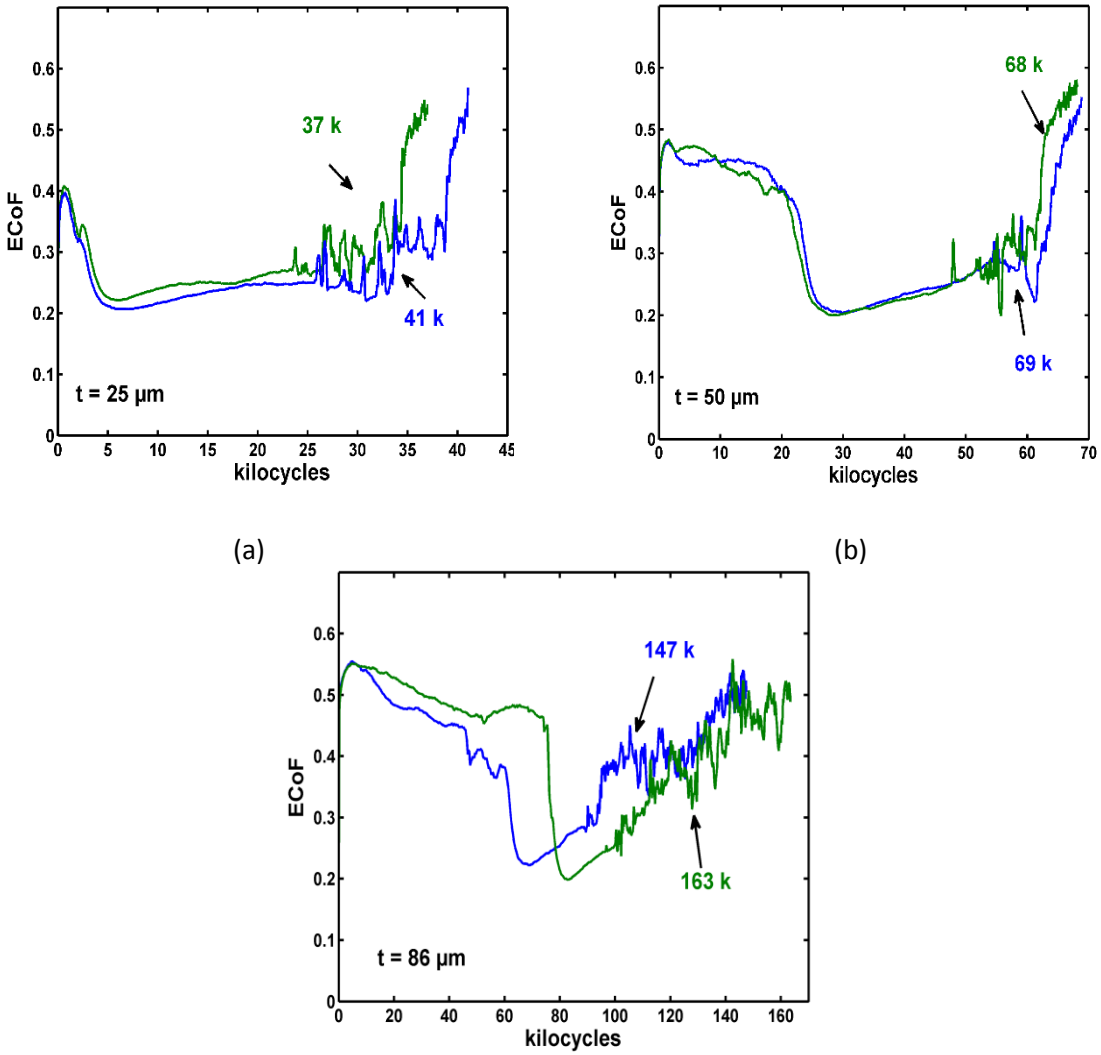

Figure 9 Repeatability of the evolution of ECoF with number of cycles for tests with R = 15 mm across the range of DFL thicknesses; (a) t = 25 µm; (b) t = 50 µm; (c) t = 86 µm.

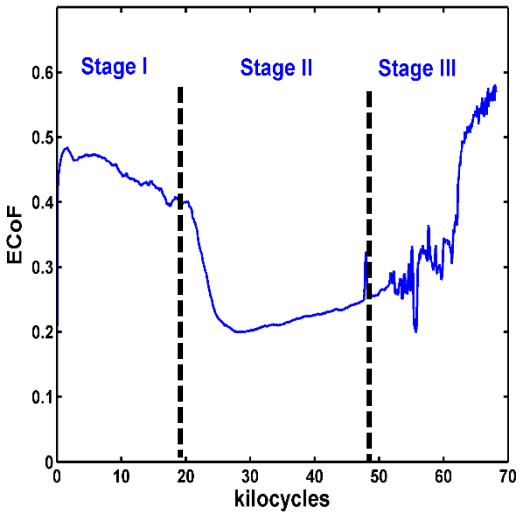

Figure 10 Evolution of ECoF with number of cycles (R = 15 mm, t = 50 µm) along with categorization into stages of behaviour.

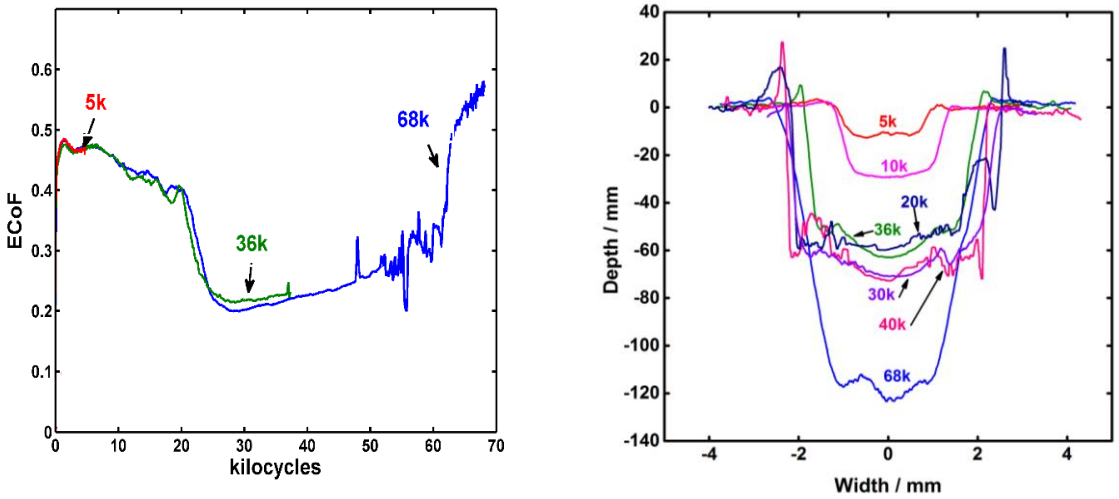

(a) (b)

Figure 11 (a) Evolution of ECoF with number of cycles (R = 15 mm, t = 50 µm) for both completed and interrupted tests (indicating the number of cycles at interruption or completion); (b) average depth profiles across the corresponding wear scars.

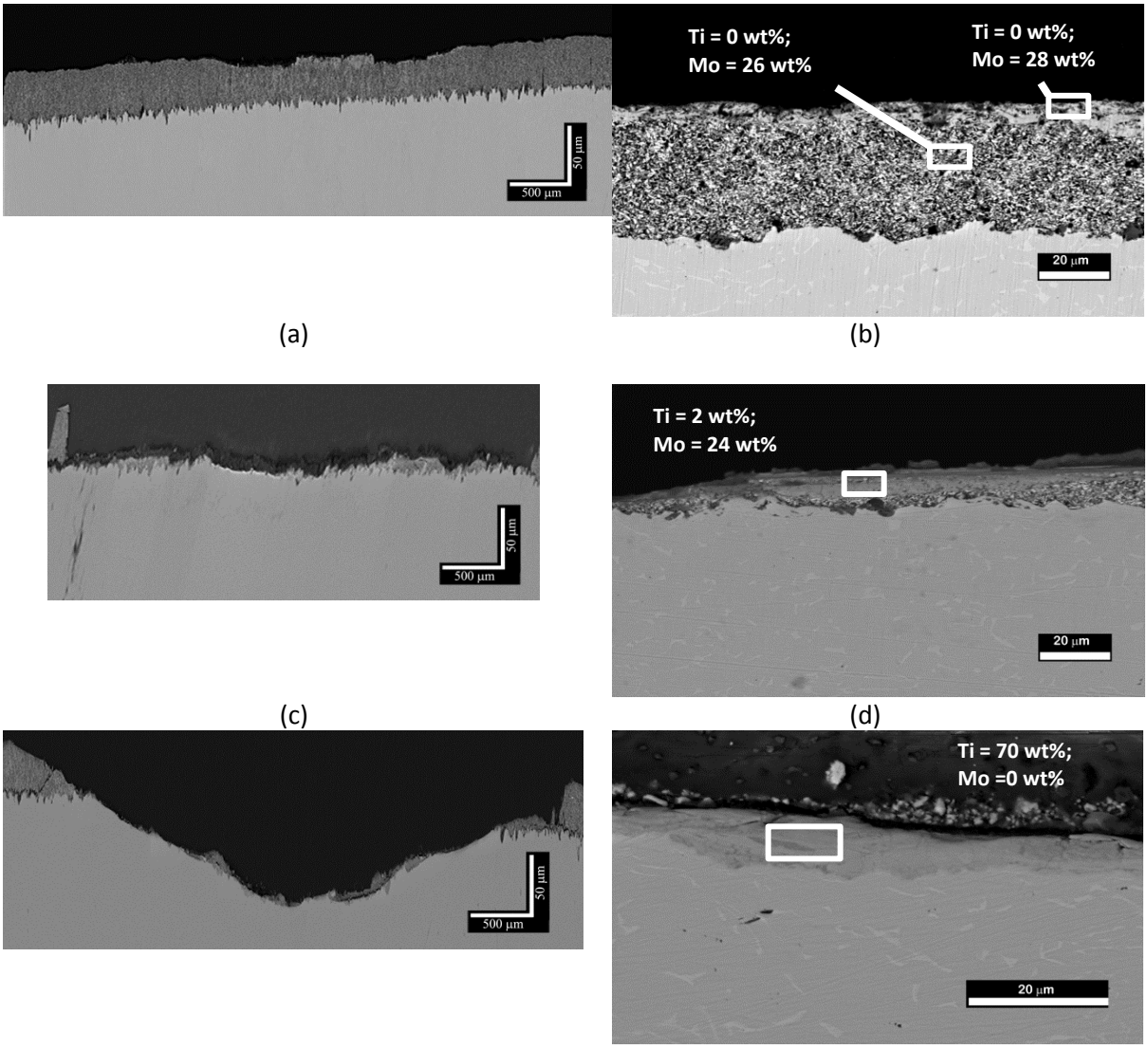

Figure 12 BSE micrographs of wear scar cross-sections (R = 15 mm, t = 50 µm) as a function of number of cycles corresponding to the tests described in Figure 11. (a), (c) and (e) are a low magnification images with a distorted aspect ratio (vertical magnification being ten times the horizontal magnification); (b), (d) and (f) are high magnification images of representative sections of the corresponding scar surface along with EDX data (elements included in the ZAF analysis: Ti, Al, V, Mo, S, C, O) representing the titanium and molybdenum contents of the areas indicated. (a) and (b) following 5 k cycles (stage I); (c) and (d) following 36k cycles (stage II); (e) and (f) following 68k cycles (stage III).

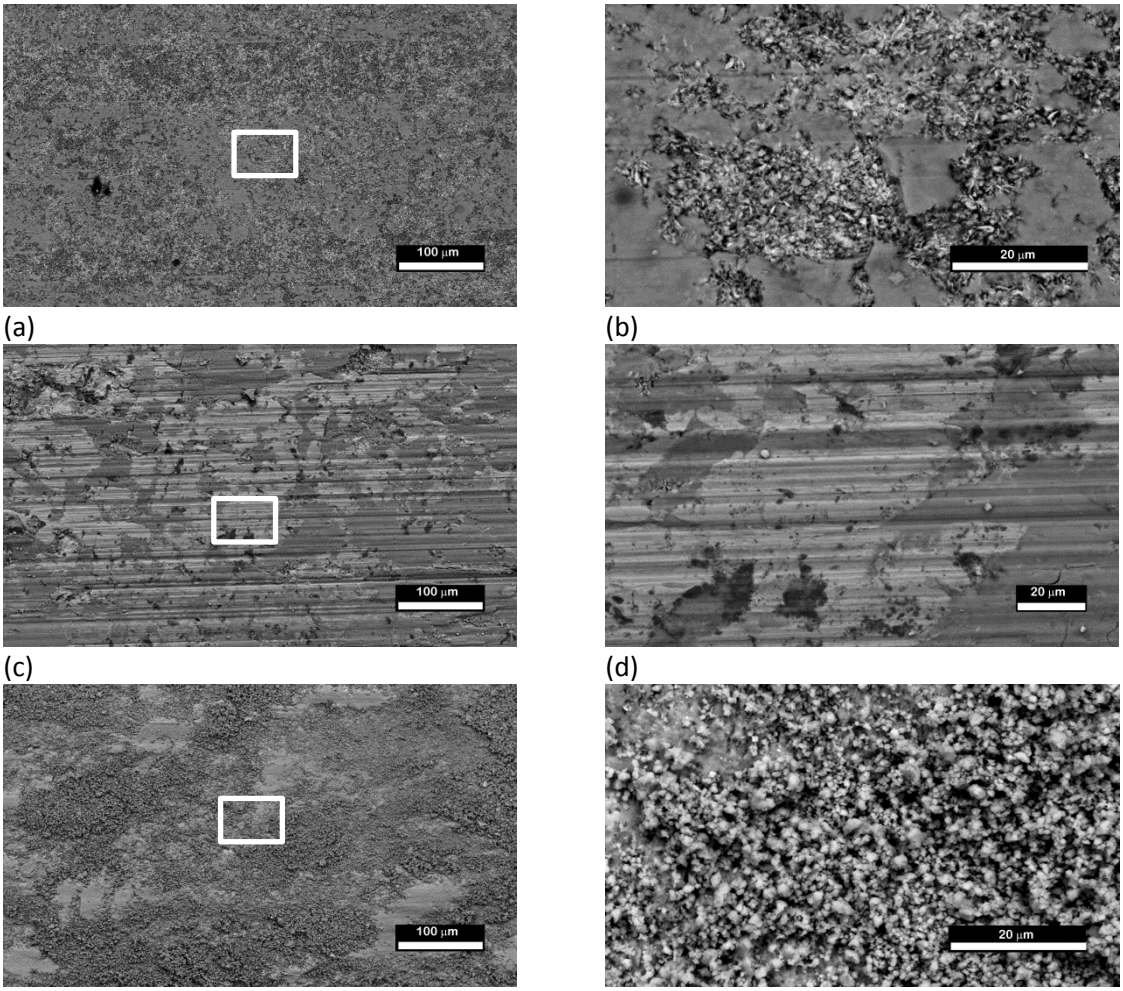

Figure 13 BSE plan view micrographs of wear scars (R = 15 mm, t = 50 µm) as a function of number of cycles corresponding to the tests described in Figure 11. (a), (c) and (e) are a low magnification images; (b), (d) and (f) are corresponding high magnification images from the regions indicated. (a) and (b) following 5 k cycles (stage I); (c) and (d) following 36k cycles (stage II); (e) and (f) following 68k cycles (stage III).

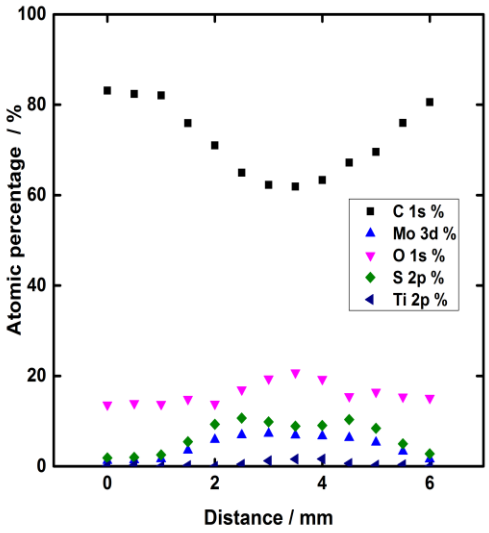

Figure 14 XPS analysis across the interrupted test wear scar (R = 15 mm, t = 50 µm) following 36k cycles (stage II), showing the atomic percentage of elements across the wear scar. Positionally, 0 mm and 6 mm are outside the scar, with the scar existing between these lateral positions.

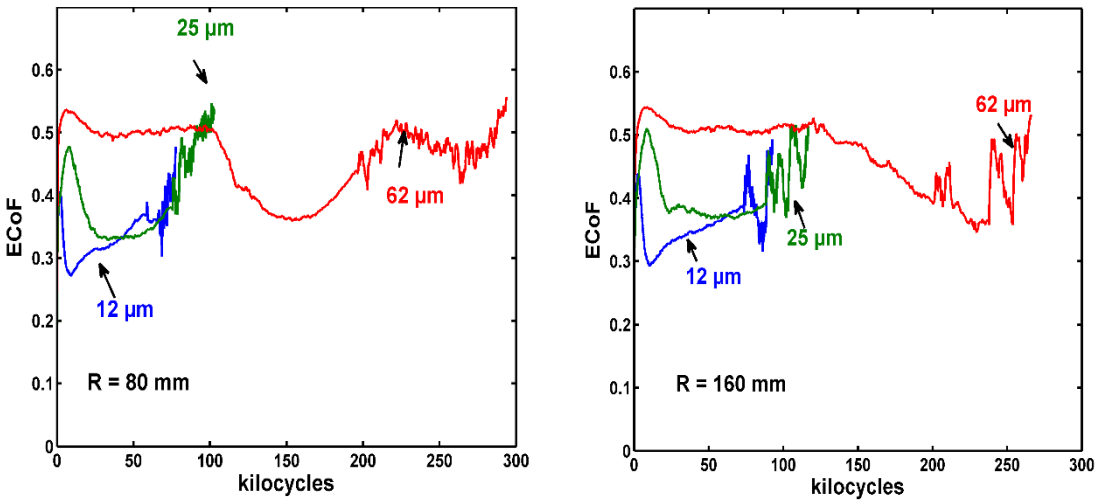

(a) (b)

Figure 15 Evolution of ECoF with number of cycles as a function of DFL thickness (t = 12 µm, 25 µm and 62 µm) for contacts with (a) R = 80 mm and (b) R = 160 mm.

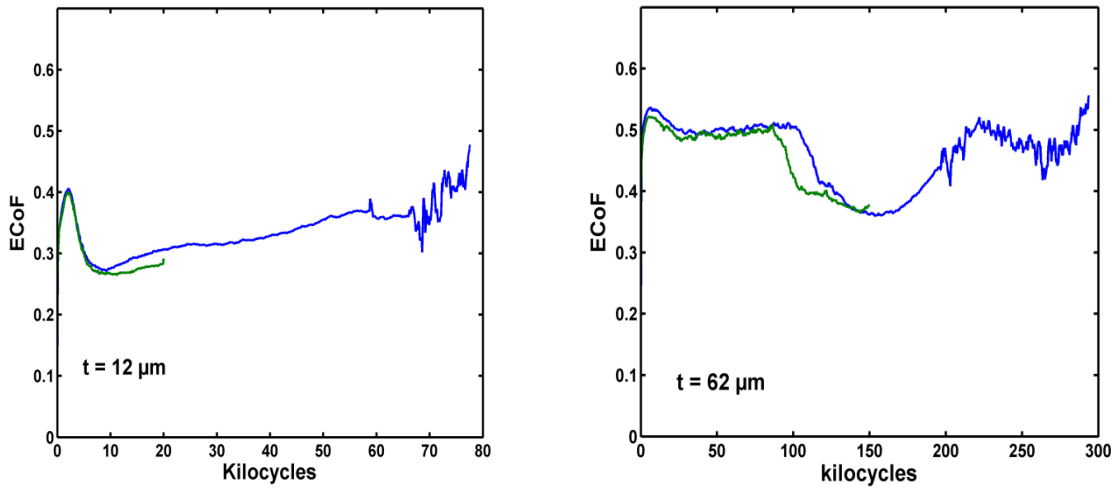

(a) (b)

Figure 16 Evolution of ECoF with number of cycles for both a full and an interrupted test for both a thin and thick DFL film; (a) t = 12 µm, R = 80 mm; (b) t = 62 µm, R = 80 mm.

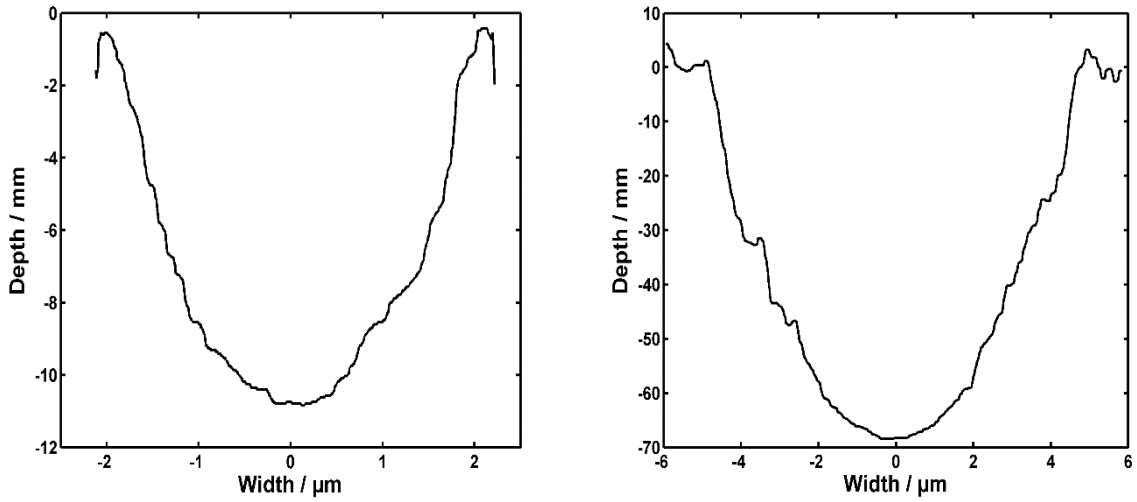

(a) (b)

Figure 17 Profilometry traces showing the wear scar dimensions at the end of the interrupted tests referred to in Figure 10; (a) t = 12 µm, R = 80 mm; (b) t = 62 µm, R = 80 mm.

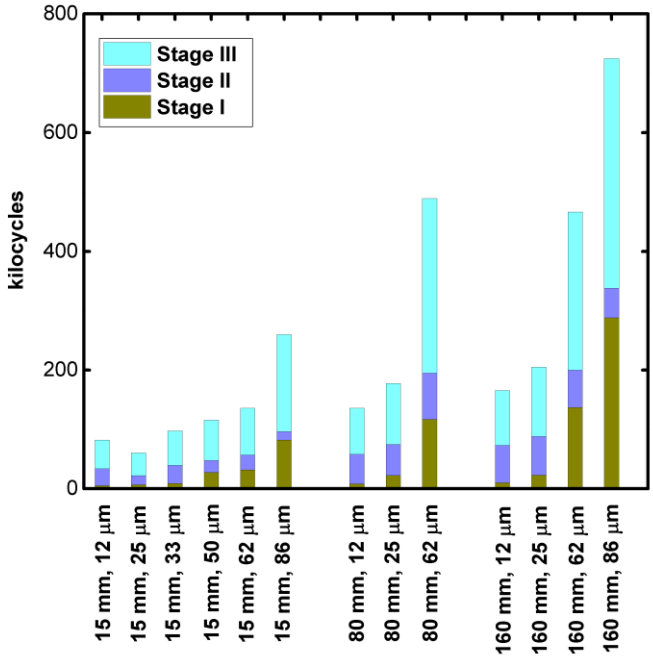

Figure 18 Histogram showing the numbers of cycles in each stage for each test configuration (cylinder radius, R and DFL thickness, t).

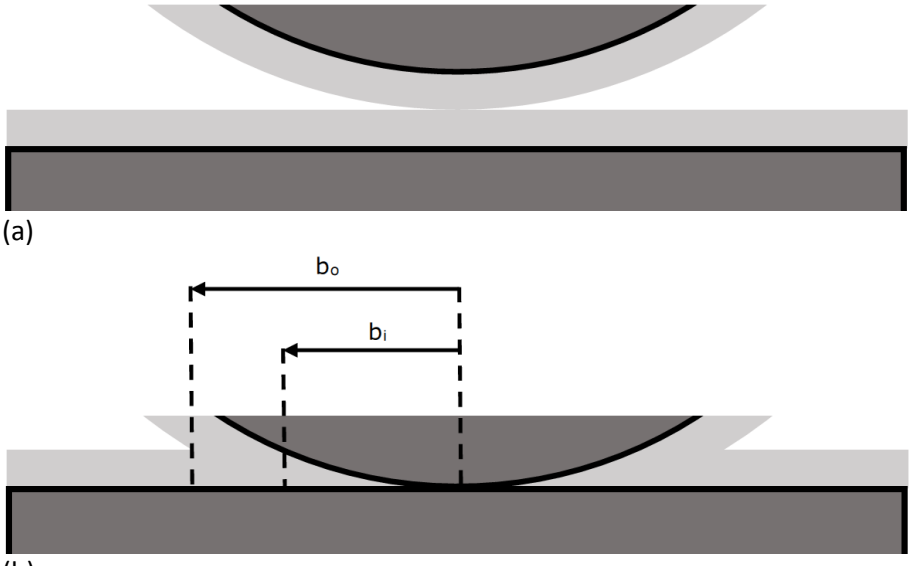

Figure 19– schematic diagram of geometrical changes take place in Stage I of the DFL wear process.

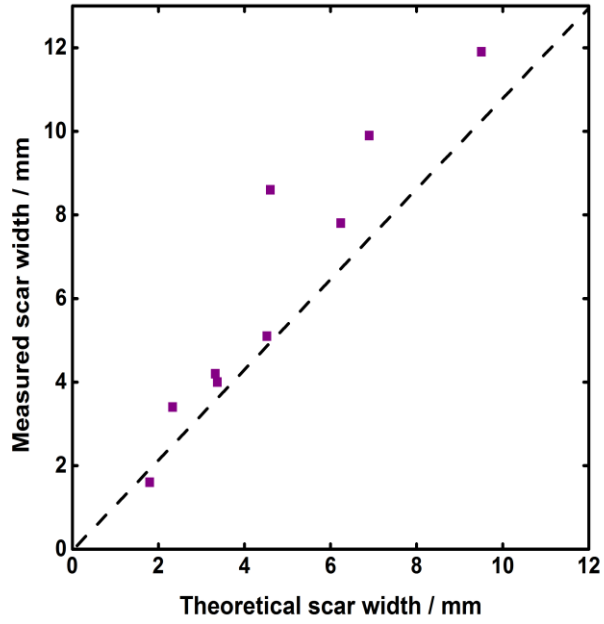

Figure 20 Comparison of theoretical and measured scar widths for tests interrupted at the end of Stage I from nine combinations of R (15, 80 and 160 mm) and t (12, 25 and 62 µm).

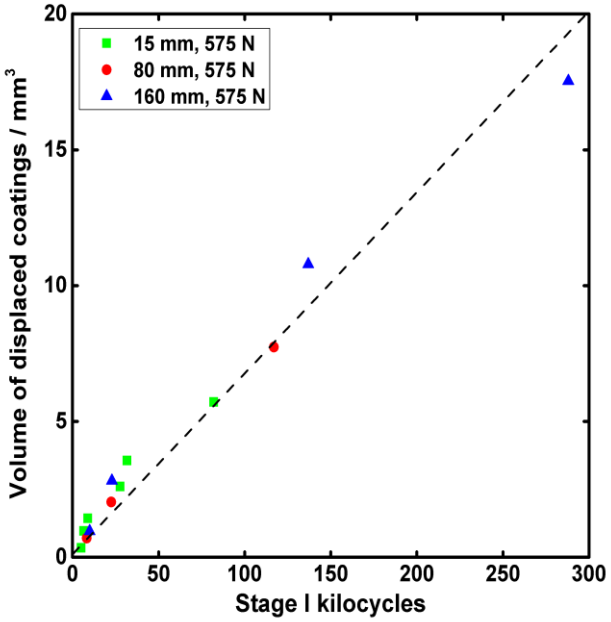

Figure 21 Volume removed in Stage I versus Stage I cycles

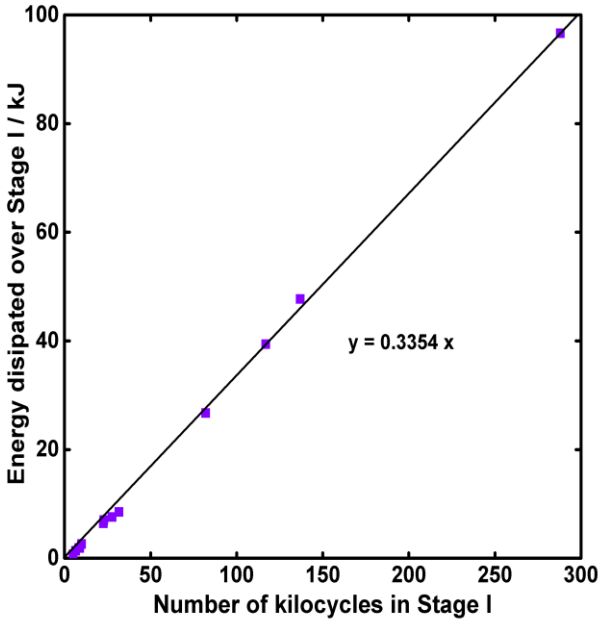

Figure 22 Total energy dissipated versus number of cycles in Stage I, for all test conditions examined

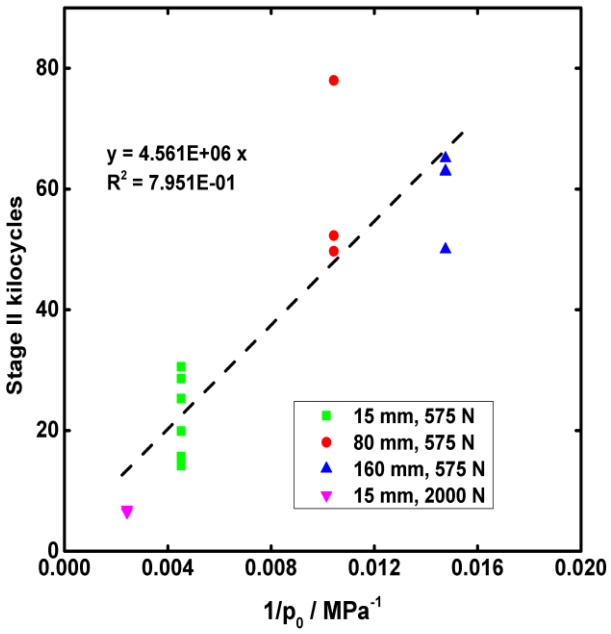

Figure 23 Stage II cycles as a function of the reciprocal of the contact pressure, p_o. Individual points represent tests with different initial DFL thicknesses.

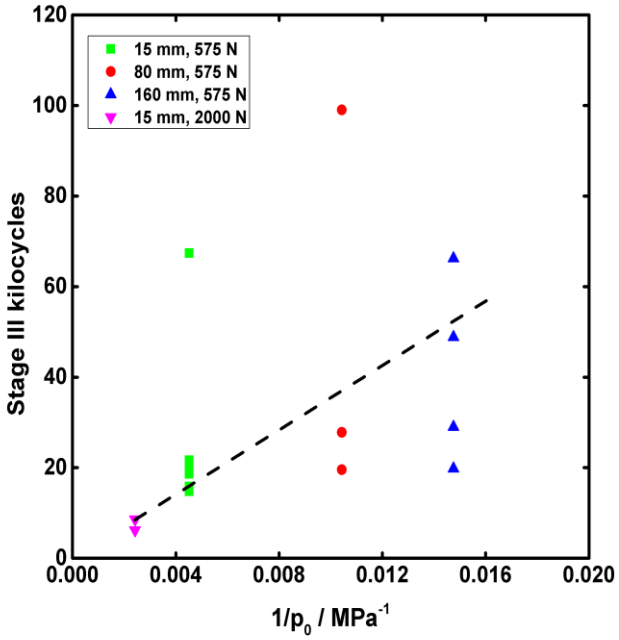

Figure 24 Stage III cycles as a function of the reciprocal of the contact pressure, p_o. Individual points represent tests with different initial DFL thicknesses.

References

[1] K. Kim, A.M. Korsunsky, Effects of imposed displacement and initial coating thickness on fretting behaviour of a thermally sprayed coating, Wear, 271 (2011) 1080-1085.
[2] D.A. Hills, Mechanics of fretting fatigue, Wear, 175 (1994) 107-113.
[3] V. Fridrici, S. Fouvry, P. Kapsa, Fretting wear behavior of a Cu–Ni–In plasma coating, Surface and Coatings Technology, 163–164 (2003) 429-434.
[4] R. Rajasekaran, D. Nowell, Fretting fatigue in dovetail blade roots: Experiment and analysis, Tribology International, 39 (2006) 1277-1285.
[5] A.M. Korsunsky, K. Kim, Dissipated energy and friction coefficient evolution during fretting wear of solid lubricant coatings, Tribology International, 43 (2010) 861-867.
[6] A.M. Korsunsky, A.R. Torosyan, K. Kim, Development and characterization of low friction coatings for protection against fretting wear in aerospace components, Thin Solid Films, 516 (2008) 5690-5699.
[7] K. Kim, A.M. Korsunsky, Dissipated energy and fretting damage in CoCrAlY-MoS2 coatings, Tribology International, 43 (2010) 676-684.
[8] S. Fouvry, V. Fridrici, C. Langlade, P. Kapsa, L. Vincent, Palliatives in fretting: A dynamical approach, Tribology International, 39 (2006) 1005-1015.
[9] P.Z. Zhen Yang, Yue Lan Di, Zhi Hai Cai, Qi Li, Investigation on Microstructure of CrN-Based Solid Self-Lubricant Composite Coating, Advanced Materials Research, 538 - 541 (2012) 406-409.
[10] C. Donnet, A. Erdemir, Historical developments and new trends in tribological and solid lubricant coatings, Surface and Coatings Technology, 180–181 (2004) 76-84.
[11] J. Xu, Z.R. Zhou, C.H. Zhang, M.H. Zhu, J.B. Luo, An investigation of fretting wear behaviors of bonded solid lubricant coatings, Journal of Materials Processing Technology, 182 (2007) 146-151.
[12] M. Dallavalle, N. Sändig, F. Zerbetto, Stability, Dynamics, and Lubrication of MoS2 Platelets and Nanotubes, Langmuir, 28 (2012) 7393-7400.
[13] J.M. Martin, Donnet, C., Le Mogne, Th., Epicier, Th, Superlubricity of molybdenum disulphide, Physical Review B, 48 (1993) 10583-10586.
[14] Y. Ye, J. Chen, H. Zhou, An investigation of friction and wear performances of bonded molybdenum disulfide solid film lubricants in fretting conditions, Wear, 266 (2009) 859-864.
[15] K. Holmberg, H. Ronkainen, A. Laukkanen, K. Wallin, S. Hogmark, S. Jacobson, U. Wiklund, R.M. Souza, P. Ståhle, Residual stresses in TiN, DLC and MoS2 coated surfaces with regard to their tribological fracture behaviour, Wear, 267 (2009) 2142-2156.
[16] K.J. Wahl, Belin, M., Singer, I. L., A triboscopic investigation of the wear and friction of MoS2 in a reciprocating sliding contact, Wear, 214 (1998) 212-220.
[17] J.M. Martin, C. Donnet, T. Le Mogne, T. Epicier, Superlubricity of molybdenum disulphide, Physical Review B, 48 (1993) 10583-10586.
[18] X. Shi, W. Zhai, Z. Xu, M. Wang, J. Yao, S. Song, Y. Wang, Synergetic lubricating effect of MoS2 and Ti3SiC2 on tribological properties of NiAl matrix self-lubricating composites over a wide temperature range, Materials & Design, 55 (2014) 93-103.
[19] T. Hu, Y. Zhang, L. Hu, Tribological investigation of MoS2 coatings deposited on the laser textured surface, Wear, 278–279 (2012) 77-82.

[20] C. Mary, Fouvry, S., Martin, J. M., Bonnet, B., Pressure and temperature effects on Fretting Wear damage of a Cu-Ni-In plasma coating versus Ti17 titanium alloy contact, Wear, 272 (2011) 18-37.
[21] J. Xu, M.H. Zhu, Z.R. Zhou, P. Kapsa, L. Vincent, An investigation on fretting wear life of bonded MoS2 solid lubricant coatings in complex conditions, Wear, 255 (2003) 253-258.
[22] X. Li, Y. Gao, J. Xing, Y. Wang, L. Fang, Wear reduction mechanism of graphite and MoS2 in epoxy composites, Wear, 257 (2004) 279-283.
[23] H. Kong, H.-G. Han, E.-S. Yoon, O.-K. Kwon, N.K. Myshkin, Evaluation of the wear life of MoS2-bonded-films in tribo-testers with different contact configuration, Wear, 215 (1998) 25-33.
[24] V. Fridrici, S. Fouvry, P. Kapsa, P. Perruchaut, Impact of contact size and geometry on the lifetime of a solid lubricant, Wear, 255 (2003) 875-882.
[25] K. Kim, A.M. Korsunsky, Exponential evolution law of fretting wear damage in low-friction coatings for aerospace components, Surface and Coatings Technology, 202 (2008) 5838-5846.
[26] S. Fouvry, C. Paulin, An effective friction energy density approach to predict solid lubricant friction endurance: Application to fretting wear, Wear, 319 (2014) 211-226.
[27] J. Luo, Zhu, M. H., Wang, Y. D., Zheng, J. F., Mo, J. L., Study on rotational fretting wear of bonded MoS2 solid lubricant coating prepared on medium carbon steel, Tribology International, 44 (2011) 1565-1570.
[28] M.H. Zhu, Z.R. Zhou, An investigation of molybdenum disulfide bonded solid lubricant coatings in fretting conditions, Surface and Coatings Technology, 141 (2001) 240-245.
[29] Z.R. Zhou, L. Vincent, Lubrication by thin polystyrene coating in fretting, Wear, 231 (1999) 179-184.
[30] C. Langlade, B. Vannes, M. Taillandier, M. Pierantoni, Fretting behavior of low-friction coatings: Contribution to industrial selection, Tribology International, 34 (2001) 49-56.
[31] A.L.M. Tobi, J. Ding, G. Bandak, S.B. Leen, P.H. Shipway, A study on the interaction between fretting wear and cyclic plasticity for Ti-6Al-4V, Wear, 267 (2009) 270-282.
[32] S. Fouvry, P. Duó, P. Perruchaut, A quantitative approach of Ti–6Al–4V fretting damage: friction, wear and crack nucleation, Wear, 257 (2004) 916-929.
[33] D.M. Mulvihill, M.E. Kartal, A.V. Olver, D. Nowell, D.A. Hills, Investigation of non-Coulomb friction behaviour in reciprocating sliding, Wear, 271 (2011) 802-816.
[34] S. Fouvry, P. Kapsa, L. Vincent, Quantification of fretting damage, Wear, 200 (1996) 186-205.
[35] E. Leidich, A. Maiwald, J. Vidner, A proposal for a fretting wear criterion for coated systems with complete contact based on accumulated friction energy density, Wear, 297 (2013) 903-910.